# Actuation of Janus Emulsion Droplets via Optothermally Induced Marangoni Forces

Sara Nagelberg,[1] Jan F. Totz,[1,2] Matthäus Mittasch,[3,4] Vishnu Sresht,[5] Lukas Zeininger,[6,7] Timothy M. Swager,[6] Moritz Kreysing,[3,8] and Mathias Kolle[1,*]

[1]*Department of Mechanical Engineering, Massachusetts Institute of Technology, Cambridge, Massachusetts 02139, USA*
[2]*Department of Mathematics, Massachusetts Institute of Technology, Cambridge, Massachusetts 02139, USA*
[3]*Max Planck Institute of Molecular Cell Biology and Genetics, 01307 Dresden, Germany*
[4]*Dewpoint Therapeutics GmbH, 01307 Dresden, Germany*
[5]*Department of Chemical Engineering, Massachusetts Institute of Technology, Cambridge, Massachusetts 02139, USA*
[6]*Department of Chemistry, Massachusetts Institute of Technology, Cambridge, Massachusetts 02139, USA*
[7]*Max Planck Institute of Colloids and Interfaces, 14476 Potsdam, Germany*
[8]*Center for Systems Biology Dresden and Cluster of Excellence Physics of Life, Technical University, 01307 Dresden, Germany*

(Received 11 May 2021; accepted 17 August 2021; published 29 September 2021)

Microscale Janus emulsions represent a versatile material platform for dynamic refractive, reflective, and light-emitting optical components. Here, we present a mechanism for droplet actuation that exploits thermocapillarity. Using optically induced thermal gradients, an interfacial tension differential is generated across the surfactant-free internal capillary interface of Janus droplets. The interfacial tension differential causes droplet-internal Marangoni flows and a net torque, resulting in a predictable and controllable reorientation of the droplets. The effect can be quantitatively described with a simple model that balances gravitational and thermal torques. Occurring in small thermal gradients, these optothermally induced Marangoni dynamics represent a promising mechanism for controlling droplet-based micro-optical components.

DOI: 10.1103/PhysRevLett.127.144503

Many microfluidic technologies, including droplet-based sorting and sensing, chemical microreactors, and tunable fluidic micro-optics, are enabled by the precise manipulation of microscale droplets [1–3]. Complex droplet morphologies, such as liquid Janus particles [4] and multiphase emulsions [5,6], are relevant in a variety of applications, including drug delivery [7,8], optics [9–11], biochemical sensors [12–15], and cosmetics [16]. Many of these applications rely on the ability to configure and optimize the droplet morphology. Since emulsion morphologies are usually stabilized with several surfactants, their configuration can be controlled by tuning the surfactant concentrations in the droplet medium or by dynamically modifying the surfactants' strength, for instance through optical stimulation [5,9]. These control mechanisms require careful tuning of the chemical environment and the design of sophisticated stimuli-responsive surfactants.

Here, we present a simple alternative for controlling emulsion droplet configuration that does not require chemical modification of the surrounding medium. The orientation of biphase emulsion droplets, formed from immiscible hydrocarbons and fluorocarbons, can be manipulated physically with a small temperature gradient generated with a focused near-infrared (NIR) laser in the fluid medium [Fig. 1(a)]. Droplets are observed to pan [see schematic in Figs. 1(b),(c)] and tilt [Figs. 1(d),(e)] as they respond to the presence and movement of the laser spot. The thermal gradient generated by the laser induces an interfacial tension gradient along the droplets' internal surfactant-free interface [Fig. 1(e)]. This interfacial tension gradient gives rise to Marangoni flows inside the droplets and a net torque, leading to droplet re-orientation. The tilt angle of the biphase emulsion droplets is determined by the balance of gravitational torque, which occurs due to the different densities of the constituent phases, and the torque associated with the optothermal Marangoni effects [Fig. 1(e)].

Thermal gradients are known to cause gradients in interfacial tension along a fluid-fluid interface [20–22]. Such gradients result in a net stress along the fluid interface causing Marangoni flows. Marangoni effects can also originate from chemical gradients, as observed in the famous tears of wine [23], and can cause emulsion droplets to act as self propelling microswimmers, driven by spontaneous symmetry breaking or optically stimulated surfactant reconfiguration [24–27]. The associated behavior of a single-phase droplet or bubble in a temperature gradient is well understood [28] and photothermal control of single phase droplets has been demonstrated in a number of microfluidic systems [29–33]. Theoretical studies of thermocapillary flows in a partially engulfed multiphase droplet show that the translation velocity of a droplet depends sensitively on its morphology and the viscosity of its constituent phases [34,35]. In experiments, the situation is further complicated due to the presence of surfactants, which are necessary for stabilizing the emulsion [36] and controlling the droplets' morphology [5].

 

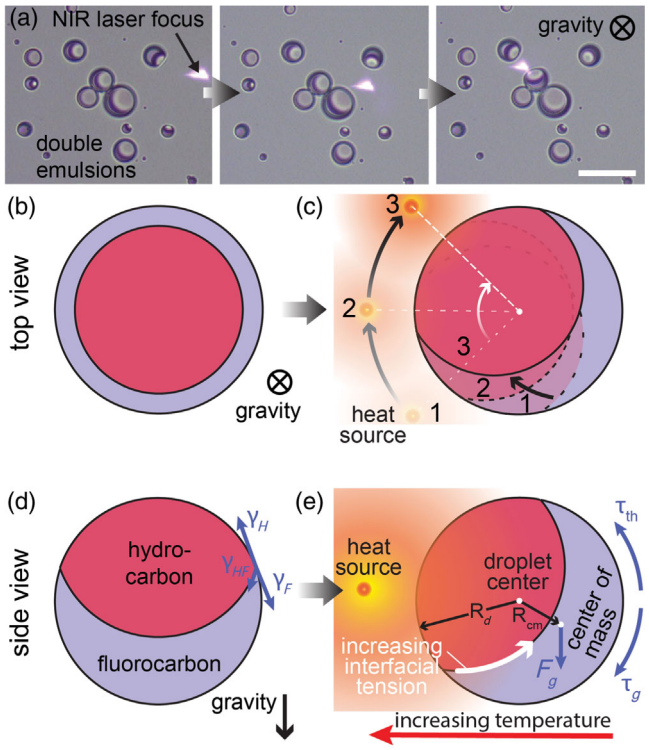


FIG. 1. Emulsion droplets reorient toward a laser spot, which acts as a localized heat source. (a) Emulsion droplets formed from heptane and perfluorohexane rotate toward the heat source; scale bar 50 $\mu$m (see video V1 in the Supplemental Material [17]). (b),(c) Top-view schematics of an emulsion droplet formed from a lighter hydrocarbon (pink) and a heavier fluorocarbon (gray) when aligned solely by gravity (b) and when a thermal source is passing by (c). (d) Side-view schematic of the same droplet, showing the relevant interfacial tensions $\gamma_H$, $\gamma_F$, and $\gamma_{FH}$. (e) The droplet's response in a thermal field, which creates an interfacial tension gradient at the droplet-internal capillary surface and results in a steady-state tilt with thermally induced torque $\tau_{th}$ and gravitational torque $\tau_g$ being balanced. $R_d$: droplet radius; $R_{cm}$: distance between center of rotation and center of mass; $F_g$: gravitational force.

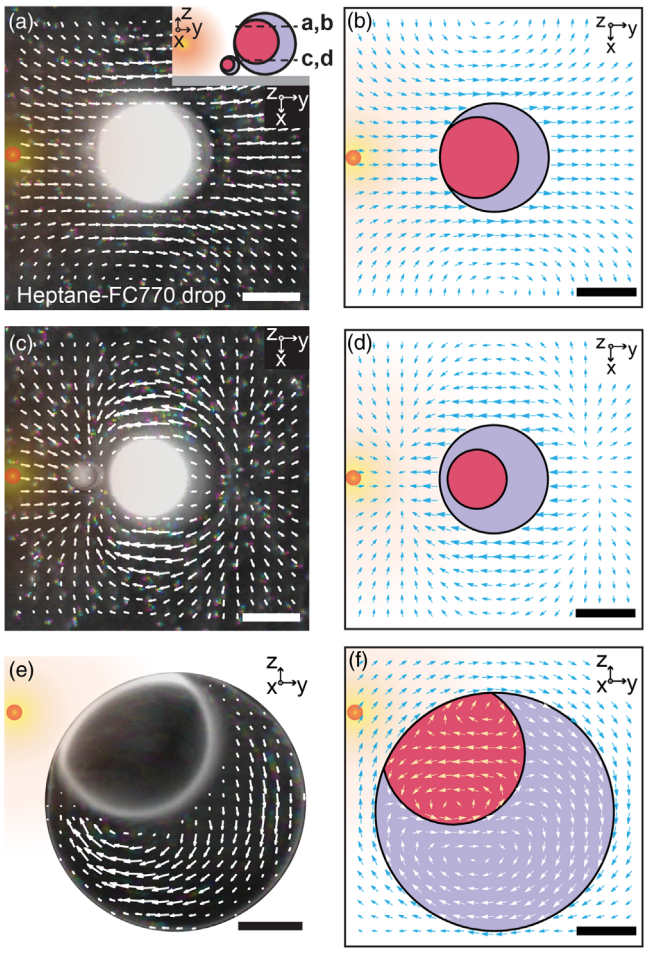


FIG. 2. Particle imaging velocimetry data and finite element modeling reveal thermocapillary flows around and in biphase droplets. (a),(c) The exterior flows, visualized in a top view, around individual heptane–FC-770 droplets at different height levels match the fields that are obtained by (b),(d) finite element modeling in the same planes. The inset in (a) locates the optical slices shown in (a)–(d). The location of the IR laser spot is marked schematically with orange dots. (e) Interior flow fields seen in the FC-770 phase of an 80 $\mu$m-sized droplet match the (f) modeled flow fields. All scale bars are 20 $\mu$m.

When subjected to a rise in temperature, surfactants may cause an increase in interfacial tension due to enhanced chemical cohesion [30], acting in opposition to conventional thermal Marangoni forces. The redistribution of surfactants on the surface will also act to mitigate any thermally induced interfacial tension gradients [37,38].

In our experiments, these various competing effects suppress interfacial tension gradients in the outer surfaces of the biphase emulsion droplets when a thermal gradient is applied. The observed Marangoni flows and the associated reorientation of the droplets is therefore primarily driven by the surfactant-free capillary interface between the two phases. This is readily apparent when comparing the clearly observable flows in and around a Janus droplet exposed to a thermal gradient (Fig. 2) with the absence of directional flows around single-phase droplets made from the emulsion's constituent phases (see the Supplemental Material [17], Fig. S1). We visualize thermally induced Marangoni flows around the emulsion droplets by dispersing fluorescent particles in the surrounding aqueous medium (see video V2 in the Supplemental Material) and map the flow fields using particle imaging velocimetry [39]. When subjected to a laser-induced thermal gradient, substantial fluid motion can be perceived in the vicinity of biphase droplets [Figs. 2(a),(c)]. The presence of a small amount of phase impurities inside some droplets allowed us to qualitatively map the flow fields in the fluorocarbon phase [Fig. 2(e)]. The experimentally observed flow patterns are closely matched by the theoretical flow fields obtained through finite element modeling [Figs. 2(b),(d),(f)], with experimentally estimated fluid velocities on internal interface and droplet surface assigned as a Dirichlet condition

(see the Supplemental Material, section II.C). Further, with the approximated flow field at the droplet interface, we find that the net force acting on the droplet vanishes (see the Supplemental Material, section II.C) [40]. Single-phase droplets composed of either emulsion phase exhibit no systematic external flow (see the Supplemental Material, Fig. S1), which indicates that the exterior droplet interfaces do not play a role in the observed dynamics. The internal interface between the two constituent phases is the critical driver for the manifestation of the observed dynamics.

To assess how the curvature of the internal capillary surface and the magnitude of the thermal differential affect the droplet dynamics, we systematically varied the distance between the laser spot and droplets with different morphologies and quantified their steady-state tilt angle $\alpha^*$ (Fig. 3). To modify the droplet morphology, we adjust the interfacial tensions between the constituent oils and the aqueous medium by changing the relative surfactant concentrations [5]. Droplets with a large internal interface curvature tilt significantly more than similarly sized droplets with a smaller interface curvature [Figs. 3(a)–(c)]. For all tested droplet configurations, the steady-state rotation angle $\alpha^*$ decreased with increasing distance between droplet and heat source [Fig. 3(d)].

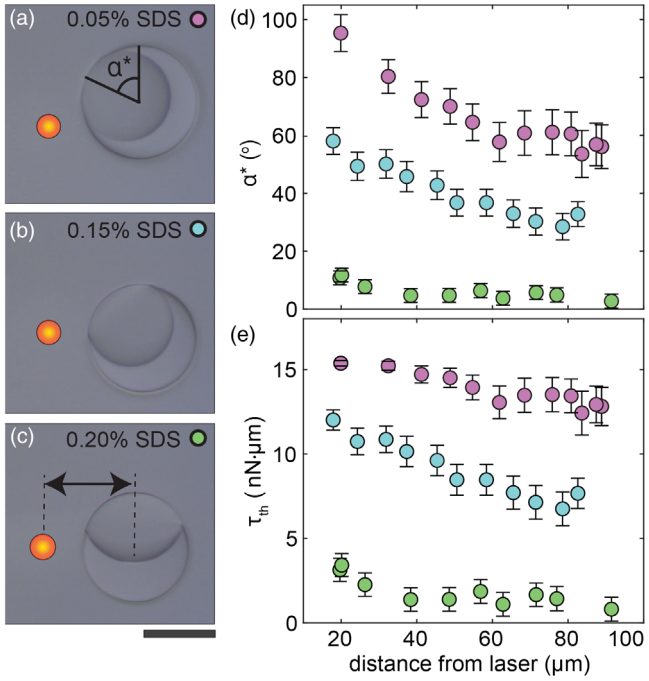


FIG. 3. Quantifying rotation in thermal gradients for different droplet morphologies. (a)–(c) Side-view images of droplets in the vicinity of a focused NIR laser in 0.4 wt% Zonyl and varying sodium dodecyl sulfate (SDS) concentrations to vary interface curvature—0.05 wt% SDS [(a), magenta], 0.15 wt% SDS [(b), cyan], 0.20 wt% SDS [(c), green]; scale bar 50 $\mu$m. (d) Steady-state rotation angle $\alpha^*$ of droplets in (a)–(c) and (e) the corresponding thermal torque $\tau_{\mathrm{th}}$ versus distance from the laser spot. Morphological droplet parameters are listed in the Supplemental Material (table S2).

For our experiments, we used Fluorinert FC-770 and heptane to form approximately spherical biphase emulsions. FC-770 has a significantly higher density ($\rho_F = 1793\ \mathrm{kg\,m^{-3}}$) than heptane ($\rho_H = 684\ \mathrm{kg\,m^{-3}}$), resulting in a pronounced torque, when the droplets' symmetry axis is not aligned with gravity. The rotation of biphase droplets in a thermal gradient is opposed by this gravitational torque. As the droplets reach the steady-state rotation angle $\alpha^*$, the thermally induced torque is balanced by the gravitational torque. The gravitational torque can be mathematically expressed as $\tau_g = R_{\mathrm{cm}} \cdot Mg \sin\alpha^*$, where $M$ is the total mass of the droplet, $g = 9.81\ \mathrm{m\,s^{-2}}$ is the gravitational constant, and $R_{\mathrm{cm}}$ is the distance from the droplet's center of rotation to its center of mass (Fig. 1(e); details provided in the Supplemental Material, section II.A). This allowed us to quantify the magnitude of the thermally induced torque as a function of droplet morphology and distance between droplets and heat source [Fig. 3(e)].

The observed dependence of the droplet rotation on the thermal differential and internal interface curvature can be captured in a simple theoretical model: to determine the optically induced thermal torque and steady-state rotation angle $\alpha^*$ for a given droplet geometry, we minimize the sum of gravitational energy $E_g(\alpha)$ and the energy $E_{\mathrm{th}}(\alpha)$ resulting from the thermally induced variation in interfacial tension across the droplet-internal capillary interface with respect to the droplet's tilt angle $\alpha$ (for a detailed discussion, see the Supplemental Material, section II.B) [41–43]. This approach is equivalent to balancing gravitational torque $\tau_g(\alpha)$ and thermally induced torque $\tau_{\mathrm{th}}(\alpha)$. The two energies can be expressed as

$$E_g(\alpha) = R_{\mathrm{cm}} M g (1 - \cos\alpha) \tag{1}$$

$$E_{\mathrm{th}}(\alpha) = \int_{\Omega_i} \gamma_{\mathrm{FH}}(T(\vec{r}, \alpha)) dA. \tag{2}$$

The shape of the curved capillary interface $\Omega_i$ between the droplet's constituent phases can be described as a spherical cap with surface area $A_i = 2\pi R_i^2 (1 - \cos\theta_i)$, where $R_i$ is the radius of curvature of the internal interface and $\theta_i$ represents the spherical cap's apex half angle (see the Supplemental Material, Fig. S4). To allow for an analytical solution, we linearize the surface tension dependence on temperature $\gamma_{\mathrm{FH}}(T) = \gamma_0 + \gamma_1 T$ and approximate the spatial temperature profile in a co-rotating droplet reference frame as $T(\vec{r}, \alpha) = T_0 + \vec{r} \cdot \vec{n}(\alpha)(\Delta T / 2R_d)$. Here, $R_d$ is the droplet radius, $\vec{r}$ the position vector measured from the droplet center, $\vec{n}(\alpha)$ the direction of the thermal gradient in the co-rotating reference frame, and $\Delta T$ the temperature differential across the droplet. The steady-state rotation angle $\alpha^*$ can then be expressed analytically as

$$\tan\alpha^* = \frac{\gamma_1 \frac{\Delta T}{2R_d} A_i [d - \frac{1}{2} R_i (1 + \cos\theta_i)]}{R_{\mathrm{cm}} M g}, \qquad (3)$$

where $d$ is a morphological parameter that describes the distance between the droplet center and the center of curvature of the internal interface (for derivations, see the Supplemental Material, sections II.A and II.B).

By applying this simple model to the experimentally studied droplet morphologies shown in Fig. 3, we recover the observed behavior qualitatively. The droplets all exhibit a very similar gravitational energy dependence on the rotation angle $\alpha$ [Fig. 4(a)], since their mass and center of gravity are very similar. However, they show an order of magnitude difference in their surface energies due to their different capillary interface curvatures [Fig. 4(b)]. This shifts the global minimum in the rotational energy landscape away from 0° toward larger tilts [Fig. 4(c)]. In agreement with experiments (where the temperature differential decreases with the distance from the laser spot), the orientation angle grows monotonically with increasing temperature differential for all shown morphologies until it saturates at 90° [Fig. 4(d)]. Correspondingly, the thermal torque grows as well [Fig. 4(e)].

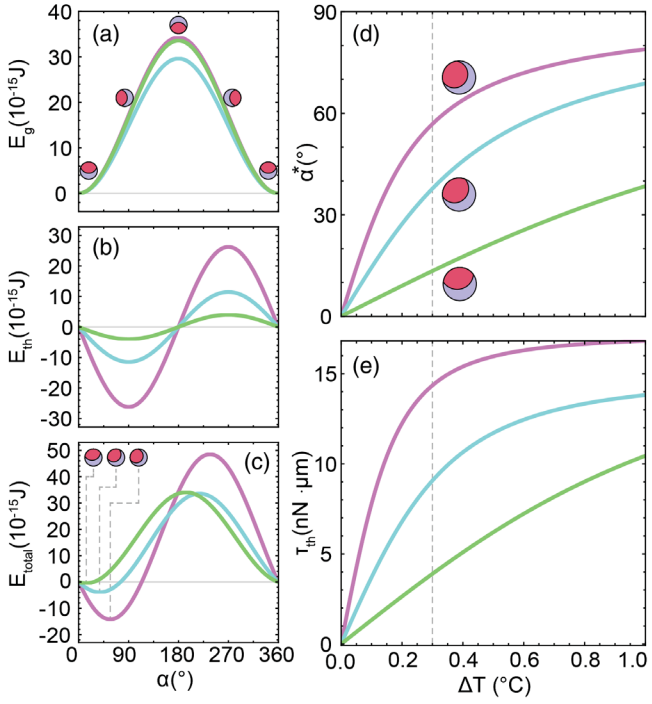


FIG. 4. Modeling of droplet response: energy balance, resulting rotation angles, and torques. (a)–(c) Potential energy $E_g$ due to gravity, energy $E_\gamma$ due to thermally induced surface tension gradient, and the sum of both versus rotation angle $\alpha$. (d),(e) Steady-state rotation angle $\alpha^*$ and thermal torque $\tau_{\mathrm{th}}$ versus temperature differential $\Delta T$ across droplet. The three differently shaded curves represent droplet geometries with increasing internal interface curvature that match the experimentally observed geometries shown in Fig. 3; $R_i = 0.82R_d$ (magenta), $R_i = 0.86R_d$ (cyan), $R_i = 0.99R_d$ (green), $\gamma_1 = -0.2$ mN m$^{-1}$ K$^{-1}$.

The droplets' dynamic response to thermal gradients is observable at a laser power of ∼50 mW without any absorption-enhancing dye in the aqueous medium. In addition, we observe small translational motion if droplets are exposed to significantly higher laser power (∼150 mW; see video V3 and Fig. S3 in the Supplemental Material), which suggests that the thermal differentials required to induce droplet rotation are significantly smaller than the temperature gradients needed for single-phase droplet manipulation [30,31].

To estimate the magnitude of the thermal gradient needed to induce droplet reorientation, we harnessed the temperature-dependent fluorescence of 2'7' dichlorofluorescein (FL27) [44,45]. Unlike other common organic dyes, whose fluorescence decreases with increasing temperature [46], FL27 exhibits increased light emission in the anti-Stokes band for higher temperatures (when excited with green light of 532 nm wavelength). This positive correlation of temperature and anti-Stokes emission can clearly be seen [Fig. 5(a)] when collecting the emitted light with a short-pass filter (cutoff at 520 nm). The short-pass filter suppresses elastically scattered light and Stokes band fluorescence, which permits optical quantification of small thermal gradients.

Knowing the dyes' emission strength as a function of temperature, we mapped the thermal field around the NIR laser focus [Fig. 5(b)]. A NIR-absorbing dye was added to the aqueous medium in these experiments in order to increase the thermal gradient so that it could be visualized with this optical technique. Therefore, the gradient measured in this experiment is significantly larger than in the previous experiment and could be used to rotate a larger droplet. Although the raw intensity data is affected by substantial pixel noise, radial averages around the laser's focal center provide a reasonable estimate of the temperature of the aqueous medium as a function of distance from the laser focus [Fig. 5(c)], which is well approximated with a simple power law (see the Supplemental Material, section I.D). This allowed us to quantify the thermal differential that the droplets were experiencing as a function of distance to the laser for various values of laser currents. With this knowledge, we quantify the correlation between the temperature differential $\Delta T$ across a droplet and its steady-state tilt [Figs. 5(d)–(f)], which we determined by side-view optical microscopy. The measured steady-state rotation angle $\alpha^*$ is used to quantify the gravitational torque, which is equal in magnitude to the thermal torque [Fig. 5(g)]. Theoretical predictions from our simple analytical model obtained by substituting the measured temperature profile in the equation of the thermal energy [Eq. (2)] are in good quantitative agreement with the experimental observations for rotation angle and torque [Figs. 5(f),(g)]. The thermal differential needed to induce

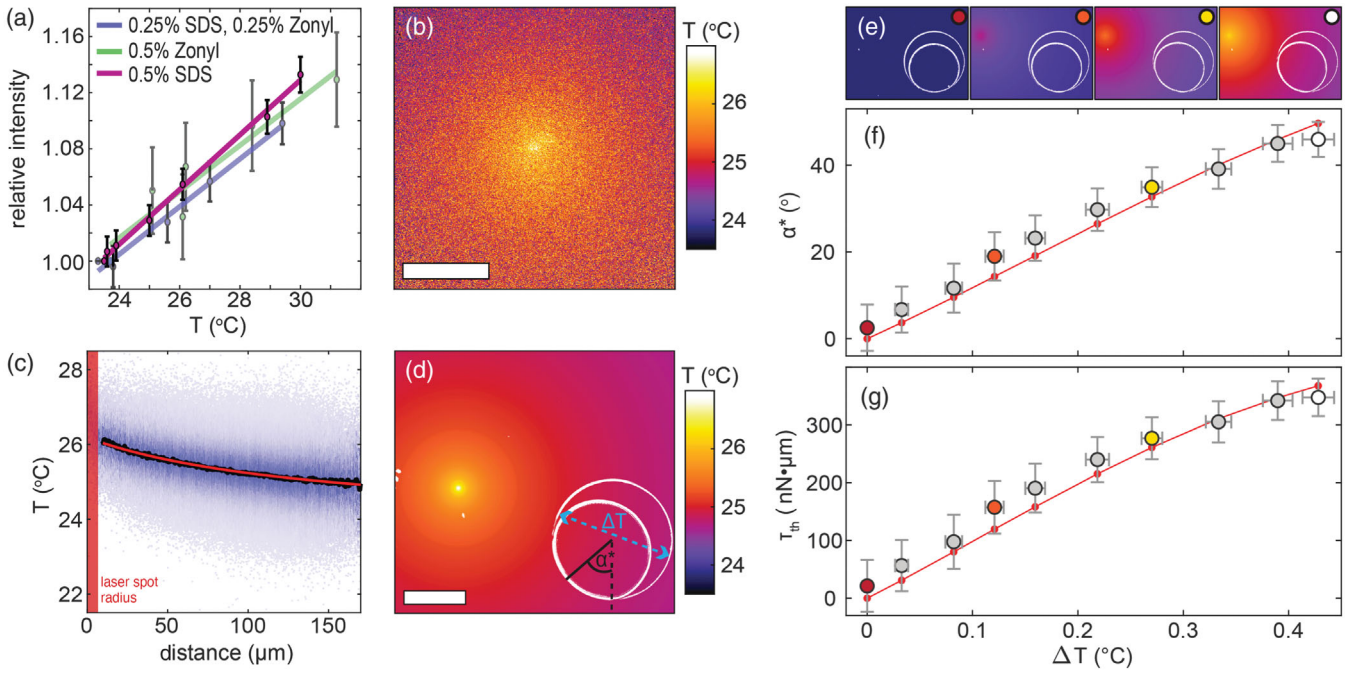


FIG. 5. Quantifying droplet rotation and torque as a function of temperature differential. (a) Temperature dependence of emission intensity of FL27 with different SDS and Zonyl surfactant concentrations in the aqueous medium relative to emission at room temperature. (b) Temperature distribution around laser measured from the relative intensity of FL27 using the fit shown in (a); scale bar: 100 $\mu$m. (c) Measured temperature (blue) as a function of distance from the laser with mean values (black) and fit (red). (d) Temperature map around laser spot using the fit shown in (c) with optical micrograph overlay of droplet; scale bar 100 $\mu$m. (e) Optical micrograph overlays of fitted temperature distribution for laser currents of 0.5 A, 0.8 A, 1.1 A, and 1.4 A. (f) Rotation of droplet as a function of temperature differential $\Delta T$ across the droplet, as shown in (d). (g) Thermal torque $\tau_{th}$ vs $\Delta T$. Data points shown in color in (f),(g) correspond to images in (e) marked with the same color. Experimental observations match the theoretically predicted behavior (red curves).

droplet rotation is smaller than 0.05 °C across the diameter of the droplet.

In summary, Janus emulsion droplets dynamically reorient in a thermal gradient. These rotations are due to thermocapillary effects occurring at the droplets' internal interface. A temperature gradient across the surfactant-free internal interface generates an interfacial tension differential that induces Marangoni-type fluid motion within the droplets, entraining flows around them. With the internal interface being the driver for the droplet reorientation, droplet morphology strongly influences the response to thermal gradients: Droplets with highly curved interfaces rotate more than those with a flatter internal capillary surface. Biphase emulsion droplets with a surfactant-free internal interface thus harbor a built-in motor that is activated via a temperature differential across the droplet. The rotational effect of thermocapillary motion in surfactant-stabilized multiphase droplets described here for the first time could prove important in microfluidic sorting, droplet mixing, microreactors, thermally controlled adaptive micro-optical systems, and optofluidic calorimetric sensors that translate microscale heat flows into optically detectable deflections of light.

We thank Professor Lauren Zarzar (Penn State University) for inspiring discussions at the start of this project. S. N. and M. K. acknowledge support by the National Science Foundation's CBET programme on "Particulate and Multiphase Processes" under Grant No. 1804241 and from the US Army Research Office through the Institute for Soldier Nanotechnologies at MIT under Contract No. W911NF-13-D-0001. J. F. T. acknowledges support through a Feodor Lynen Fellowship of the Alexander von Humboldt Foundation. M. Kr. acknowledges support from the European Research Council, Grant No. 853619 (GHOSTs). This research was supported in part by a Vannevar Bush Faculty Fellowship to T. M. S. (Grant No. N000141812878). L. Z. acknowledges support through a fellowship of the German Research Foundation (DFG), Grant No. ZE1121/1-1, and a DFG Emmy Noether grant, Grant No. ZE1121/3-1.

S. N. and J. F. T contributed equally to this work.

*Corresponding author.
mkolle@mit.edu

[1] H.-D. Xi, H. Zheng, W. Guo, A. M. Gañán-Calvo, Y. Ai, C.-W. Tsao, J. Zhou, W. Li, Y. Huang, N.-T. Nguyen, and S. Hwa Tan, Active droplet sorting in microfluidics: a review, Lab Chip **17**, 751 (2017).

[2] L. Liu, N. Xiang, and Z. Ni, Droplet-based microreactor for the production of micro/nano-materials, Electrophoresis **41**, 833 (2020).

[3] H. Zappe, *Fundamentals of Micro-Optics* (Cambridge University Press, Cambridge, England, 2010), https://doi.org/10.1017/CBO9780511781797.

[4] T. Nisisako, Recent advances in microfluidic production of Janus droplets and particles, Curr. Opin. Colloid Interface Sci. **25**, 1 (2016).

[5] L. D. Zarzar, V. Sresht, E. M. Sletten, J. A. Kalow, D. Blankschtein, and T. M. Swager, Dynamically reconfigurable complex emulsions via tunable interfacial tensions, Nature **518**, 520 (2015).

[6] T. Sheth, S. Seshadri, T. Prileszky, and M. E. Helgeson, Multiple nanoemulsions, Nat. Rev. Mater. **5**, 214 (2020).

[7] M. A. Augustin and Y. Hemar, Nano- and micro-structured assemblies for encapsulation of food ingredients, Chem. Soc. Rev. **38**, 902 (2009).

[8] C.-X. Zhao, Multiphase flow microfluidics for the production of single or multiple emulsions for drug delivery, Adv. Drug Delivery Rev. **65**, 1420 (2013).

[9] S. Nagelberg, L. D. Zarzar, N. Nicolas, K. Subramanian, J. A. Kalow, V. Sresht, D. Blankschtein, G. Barbastathis, M. Kreysing, T. M. Swager, and M. Kolle, Reconfigurable and responsive droplet-based compound micro-lenses, Nat. Commun. **8**, 14673 (2017).

[10] A. E. Goodling, S. Nagelberg, B. Kaehr, C. H. Meredith, S. I. Cheon, A. P. Saunders, M. Kolle, and L. D. Zarzar, Colouration by total internal reflection and interference at microscale concave interfaces, Nature **566**, 523 (2019).

[11] A. E. Goodling, S. Nagelberg, M. Kolle, and L. D. Zarzar, Tunable and responsive structural color from polymeric microstructured surfaces enabled by interference of totally internally reflected light, ACS Mater. Lett. **2**, 754 (2020).

[12] T. M. Swager, Sensor technologies empowered by materials and molecular innovations, Angew. Chem. Int. Ed. **57**, 4248 (2018).

[13] Q. Zhang, S. Savagatrup, P. Kaplonek, P. H. Seeberger, and T. M. Swager, Janus emulsions for the detection of bacteria, ACS Cent. Sci. **3**, 309 (2017).

[14] L. D. Zarzar, J. A. Kalow, X. He, J. J. Walish, and T. M. Swager, Optical visualization and quantification of enzyme activity using dynamic droplet lenses, Proc. Natl. Acad. Sci. U.S.A. **114**, 3821 (2017).

[15] L. Zeininger, S. Nagelberg, K. S. Harvey, S. Savagatrup, M. B. Herbert, K. Yoshinaga, J. A. Capobianco, M. Kolle, and T. M. Swager, Rapid detection of Salmonella enterica via directional emission from carbohydrate-functionalized dynamic double emulsions, ACS Cent. Sci. **5**, 789 (2019).

[16] V. B. Patravale and S. D. Mandawgade, Novel cosmetic delivery systems: an application update, Int. J. Cosmet. Sci. **30**, 19 (2008).

[17] See Supplemental Material, which includes Refs. [18,19], at http://link.aps.org/supplemental/10.1103/PhysRevLett.127.144503 for details on experimental measurement procedures and detailed theoretical derivations.

[18] J. Schindelin, I. Arganda-Carreras, E. Frise, V. Kaynig, M. Longair, T. Pietzsch, S. Preibisch, C. Rueden, S. Saalfeld, B. Schmid, J.-Y. Tinevez, D. J. White, V. Hartenstein, K. Eliceiri, P. Tomancak, and A. Cardona, Fiji: an open-source platform for biological-image analysis, Nat. Methods **9**, 676 (2012).

[19] B. McClain, M. Yoon, J. Litster, and S. Mochrie, Interfacial roughness in a near-critical binary fluid mixture, Eur. Phys. J. B **10**, 45 (1999).

[20] S. H. Davis, Thermocapillary instabilities, Annu. Rev. Fluid Mech. **19**, 403 (1987).

[21] *Interfacial Phenomena and the Marangoni Effect*, edited by M. G. Velarde and R. K. Zeytounian, CISM International Centre for Mechanical Sciences Vol. 428 (Springer, Vienna, 2002), https://doi.org/10.1007/978-3-7091-2550-2.

[22] C. N. Baroud, Thermocapillarity, in *Encyclopedia of Microfluidics and Nanofluidics*, edited by D. Li (Springer, New York, 2013), pp. 1–7, https://doi.org/10.1007/978-1-4614-5491-5_1567.

[23] J. Thomson, On certain curious motions observable at the surfaces of wine and other alcoholic liquors, London Edinburgh Dublin Philos. Mag. **10**, 330 (1855).

[24] M. Schmitt and H. Stark, Marangoni flow at droplet interfaces, Phys. Fluids **28**, 012106 (2016).

[25] B. V. Hokmabad, K. A. Baldwin, C. Krüger, C. Bahr, and C. C. Maass, Topological Stabilization and Dynamics of Self-Propelling Nematic Shells, Phys. Rev. Lett. **123**, 178003 (2019).

[26] A. Diguet, R.-M. Guillermic, N. Magome, A. Saint-Jalmes, Y. Chen, K. Yoshikawa, and D. Baigl, Photomanipulation of a droplet by the chromocapillary effect, Angew. Chem. **48**, 9281 (2009).

[27] P. Illien, R. Golestanian, and A. Sen, 'Fuelled' motion: phoretic motility and collective behaviour of active colloids, Chem. Soc. Rev. **46**, 5508 (2017).

[28] N. O. Young, J. S. Goldstein, and M. J. Block, The motion of bubbles in a vertical temperature gradient, J. Fluid Mech. **6**, 350 (1959).

[29] M. Muto, M. Yamamoto, and M. Motosuke, A noncontact picolitor droplet handling by photothermal control of interfacial flow, Anal. Sci. **32**, 49 (2016).

[30] B. J. Won, W. Lee, and S. Song, Estimation of the thermocapillary force and its applications to precise droplet control on a microfluidic chip, Sci. Rep. **7**, 3062 (2017).

[31] W. Hu and A. T. Ohta, Aqueous droplet manipulation by optically induced Marangoni circulation, Microfluid. Nanofluid. **11**, 307 (2011).

[32] C. N. Baroud, J.-P. Delville, F. Gallaire, and R. Wunenburger, Thermocapillary valve for droplet production and sorting, Phys. Rev. E **75**, 046302 (2007).

[33] M. Robert de Saint Vincent, R. Wunenburger, and J.-P. Delville, Laser switching and sorting for high speed digital microfluidics, Appl. Phys. Lett. **92**, 154105 (2008).

[34] D. S. Morton, R. S. Subramanian, and R. Balasubramaniam, The migration of a compound drop due to thermocapillarity, Phys. Fluids A **2**, 2119 (1990).

[35] L. Rosenfeld, O. M. Lavrenteva, and A. Nir, On the thermocapillary motion of partially engulfed compound drops, J. Fluid Mech. **626**, 263 (2009).

[36] J.-C. Baret, Surfactants in droplet-based microfluidics, Lab Chip **12**, 422 (2012).

[37] J. Chen and K. J. Stebe, Surfactant-induced retardation of the thermocapillary migration of a droplet, J. Fluid Mech. **340**, 35 (1997).

[38] H. S. Kim and R. S. Subramanian, Thermocapillary migration of a droplet with insoluble surfactant: I. Surfactant cap, J. Colloid Interface Sci. **127**, 417 (1989).

[39] C. M. Leong, Y. Gai, and S. K. Y. Tang, Internal flow inside droplets within a concentrated emulsion during droplet rearrangement, Phys. Fluids **30**, 032002 (2018).

[40] E. Lauga and T. R. Powers, The hydrodynamics of swimming microorganisms, Rep. Prog. Phys. **72**, 096601 (2009).

[41] B. J. Park and D. Lee, Equilibrium orientation of nonspherical Janus particles at fluid–fluid interfaces, ACS Nano **6**, 782 (2012).

[42] H. Rezvantalab and S. Shojaei-Zadeh, Capillary interactions between spherical Janus particles at liquid–fluid interfaces, Soft Matter **9**, 3640 (2013).

[43] A. T. Oratis, T. P. Farmer, and J. C. Bird, Capillary induced twisting of Janus cylinders, Soft Matter **13**, 7556 (2017).

[44] C. E. Estrada-Pérez, Y. A. Hassan, and S. Tan, Experimental characterization of temperature sensitive dyes for laser induced fluorescence thermometry, Rev. Sci. Instrum. **82**, 074901 (2011).

[45] J. A. Sutton, B. T. Fisher, and J. W. Fleming, A laser-induced fluorescence measurement for aqueous fluid flows with improved temperature sensitivity, Exp. Fluids **45**, 869 (2008).

[46] M. C. J. Coolen, R. N. Kieft, C. C. M. Rindt, and A. A. van Steenhoven, Application of 2-D LIF temperature measurements in water using a Nd : YAG laser, Exp. Fluids **27**, 420 (1999).